# Transport phenomena in a three-dimensional system close to the magnetic quantum critical point: The conserving approximation with current vertex corrections

Seiichiro Onari,[1] Hiroshi Kontani,[2] and Yukio Tanaka[1]
[1]*Department of Applied Physics, Nagoya University, Chikusa, Nagoya 464-8603, Japan*
[2]*Department of Physics, Nagoya University, Chikusa, Nagoya 464-8603, Japan*
(Received 29 November 2005; revised manuscript received 20 April 2006; published 26 June 2006)

It is known that various transport coefficients strongly deviate from conventional Fermi-liquid behaviors in many electron systems which are close to antiferromagnetic (AF) quantum critical points (QCP). For example, Hall coefficients and Nernst coefficients in three-dimensional heavy fermion $CeCoIn_5$ and $CeCu_{6-x}Au_x$ increase strikingly at low temperatures, whose overall behaviors are similar to those in high-$T_c$ cuprates. These temperature dependencies are too strong to explain in terms of the relaxation time approximation. To elucidate the origin of these anomalous transport phenomena in three-dimensional systems, we study the current vertex corrections (CVC) based on the fluctuation exchange approximation, and find out the decisive role of the CVC. The main finding of the present paper is that the Hall coefficient and the Nernst coefficient strongly increase thanks to the CVC in the vicinity of the AF QCP, irrespective of dimensionality. We also study the relaxation time of quasiparticles, and find that "hot points" and "cold lines" are formed in general three-dimensional systems due to strong AF fluctuations.

DOI: 10.1103/PhysRevB.73.224434 PACS number(s): 72.10.Bg

## I. INTRODUCTION

Strongly correlated electron systems close to the quantum critical point (QCP) have stimulated much interest. In particular, the heavy fermion compound $CeCoIn_5$,[1] which is a three-dimensional metal close to the antiferromagnetic (AF) QCP, attracts much attention because of the non-Fermi-liquid normal state and the *d*-wave superconductivity ($T_c=2.3$ K). Moreover, recent experimental efforts have revealed the existence of interesting anomalous transport phenomena characteristic of the AF QCP. In the normal state of $CeCoIn_5$, for example, it is observed that the resistivity[2] $\rho \propto T$, the Hall coefficient[2] $R_H \propto 1/T$, and the Nernst coefficient[3] $\nu \propto 1/T$ below 20 K until $T_c=2.3$ K. These behaviors are quite different from the normal Fermi-liquid behaviors, $\rho \propto T^2$ and $R_H \propto T^0$.

In Ce115, the maximum values of $R_H$ and $\nu$ are quite huge compared to values for high temperatures. The maximum value of $R_H$ becomes about 30 times larger than the values at high temperatures. The value of $\nu$ reaches $-1.0$ $\mu$V/KT at 5 K, whose magnitude is about 1000 times larger than the values in usual metals. The temperature dependence of $R_H$ is similar to the two-dimensional high-$T_c$ cuprates above the pseudogap temperatures, and that of $\nu$ is similar to electron doped high-$T_c$ cuprates, irrespective of signs. Moreover, the magnitude of $R_H$ and $\nu$ in $CeCoIn_5$ is much larger than that in high-$T_c$ cuprates. Similar drastic increases of $R_H$ are also observed in $CeCu_{6-x}Au_x$ (Ref. 4) and $YbRh_2Si_2$,[5] which are three-dimensional heavy fermion compounds close to the AF QCP.

The relaxation time approximation (RTA)[6,7] has been used frequently in the study of transport phenomena, although its reliability for strongly correlated systems is not assured. According to the spin fluctuation theory, the relaxation time $\tau_{\boldsymbol{k}}$ becomes strongly anisotropic.[6,8] The spots on the Fermi surface where $\tau_{\boldsymbol{k}}$ takes the maximum (minimum) value is denoted by the cold (hot) spots in the literature. The ratio of the relaxation time at cold spots and hot spots $r=\tau_{\rm cold}/\tau_{\rm hot}$ and the weight of the cold spots play an important role in the transport phenomena. However, in terms of the RTA, an unrealistic huge $r$ (say $r=100-1000$) is required to reproduce the experimental enhancement of $R_H$ in $CeCoIn_5$.[2] If we assume that $R_H$ is enhanced by this mechanism, $R_H$ should be suppressed quite sensitively by a very small amount of impurity. In addition, when $r \gg 1$, the magnetoresistance should be too large to explain the modified Kohler's rule, $\Delta\rho/\rho \propto R_H^2/\rho^2$, which is observed in high-$T_c$ cuprates[9,10] and in $CeCoIn_5$.[2]

These anomalous transport phenomena close to the AF QCP are well reproduced by taking into account the current vertex corrections (CVC). Actually, the CVC is necessary to satisfy conservation laws. In the Fermi liquid theory, the CVC corresponds to the backflow, which naturally arises from electron-electron correlations. Then, the CVC is indispensable to calculate the transport coefficients in the strongly correlated electron systems, where electron-electron correlations are dominant. For example, the modified Kohler's rule is explained due to the CVC caused by the AF fluctuations.[11] The negative $R_H$ in electron doped high-$T_c$ cuprates, which cannot be explained by the RTA because the Fermi surface is hole-like everywhere, is explained if we take the CVC. Moreover, it is not easy to explain the enhancement of $\nu$ by the RTA because the Sondheimer cancellation[12] makes $\nu$ small. The enhancement of $\nu$ in electron-doped (hole-doped) high-$T_c$ cuprates is caused by the CVC due to the AF (AF and superconducting) fluctuations.

Until now, various non-Fermi-liquid behaviors of high-$T_c$ cuprates have been explained by the spin fluctuation model, such as the self-consistent renormalization (SCR) theory[13–15] and the fluctuation exchange (FLEX) theory.[16–18] For example, an appropriate behavior of the spin susceptibility and the AF correlation length $\xi$ ($\xi^2 \propto 1/T$) are obtained. Moreover, spin-fluctuation theories[6,15] derive the relation $\rho \propto T^2\xi^2$, which is consistent with the non-Fermi-liquid behaviors of high-$T_c$ cuprates close to the AF QCP. Based on the spin

 

fluctuation theory, Kontani *et al.*[11,19–21] have developed a theory of transport phenomena, by focusing on the crucial role of the CVC. This framework naturally reproduces the temperature dependence of transport coefficients for high-$T_c$ cuprates and other two-dimensional (2D) systems[22] close to the QCP.

In high-$T_c$ cuprates,[19] the CVC plays an important role on transport phenomena. However, it is highly nontrivial whether the CVC is significant in three-dimensional systems, since the CVC totally vanishes in the dynamical mean field theory (DMFT) where $d=\infty$ limit is taken.[23,24] The reason is that the irreducible four-point vertex $\Gamma^I$ in the DMFT becomes a local function, which cannot contribute to the CVC. Although it is generally believed that the DMFT works well in various three-dimensional (3D) systems with strong correlation,[23] the momentum dependencies of the self-energy and the vertex corrections are significant near the QCP. However, we must consider the CVC which cannot be taken into account within the DMFT. To elucidate this issue, we study the role of the CVC based on the AF fluctuation theory in 3D systems.

The purpose of this paper is to examine whether non-Fermi-liquid behaviors in 3D systems can be explained by taking account of the CVC in terms of the FLEX approximation. In 3D systems, massive calculation resource and time are needed to perform the calculation. We show that striking increase of $R_H$ and $\nu$ can be obtained at low temperatures even in 3D by virtue of the CVC, which is consistent with experiments in $CeCoIn_5$ and $CeCu_{6-x}Au_x$. The present study is the first microscopic calculation for the Hall coefficient and the Nernst coefficient in 3D with the CVC. We also find that in 3D systems, the hot and cold spots form point-like ("hot points") and line-like shape ("cold lines"), respectively. The CVC on the cold lines plays a major role for increasing $R_H$ and $\nu$.

## II. FORMULATION

### A. Model

We first introduce the three-dimensional Hubbard model,

$$\mathcal{H} = -\sum_{i,j}\sum_{\sigma} t_{ij} c_{i\sigma}^{\dagger} c_{j\sigma} + \frac{1}{2}\sum_{i,\sigma} U n_{i\sigma} n_{i-\sigma}, \tag{1}$$

on a stacked square lattice with the Coulomb repulsion $U$ and the intralayer hopping $t_1$, $t_2$, $t_3$ and the interlayer hopping $t_z$ depicted in Fig. 1. Hereafter, we take $t_1=1$ as a unit of energy.

Then, the dispersion is derived as

$$\epsilon_{\boldsymbol{k}}^0 = -2t_1(\cos(k_x)+\cos(k_y)) - 4t_2\cos(k_x)\cos(k_y) - 2t_3(\cos(2k_x)+\cos(2k_y)) - 2t_z\cos(k_z). \tag{2}$$

We apply the FLEX approximation[16,17,25,26] where the Green's function, the self-energy, and the susceptibility are obtained self-consistently. The FLEX approximation belongs to "conserving approximations" formulated by Baym and Kadanoff.[27,28] The spin ($\chi_{\mathbf{q}}^s$) and charge ($\chi_{\mathbf{q}}^c$) susceptibilities are

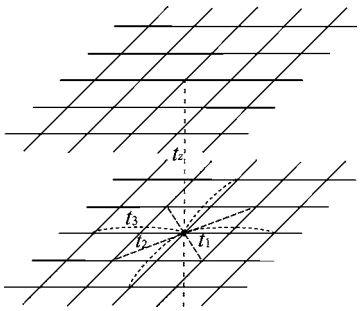


FIG. 1. The lattice structure with the nearest intralayer hopping $t_1$, the second one $t_2$, the third one $t_3$, and the interlayer hopping $t_z$.

$$\chi_{\boldsymbol{q}}^s(\omega_l) = \frac{\chi_{\boldsymbol{q}}^0(\omega_l)}{1 - U\chi_{\boldsymbol{q}}^0(\omega_l)}, \tag{3}$$

$$\chi_{\boldsymbol{q}}^c(\omega_l) = \frac{\chi_{\boldsymbol{q}}^0(\omega_l)}{1 + U\chi_{\boldsymbol{q}}^0(\omega_l)}, \tag{4}$$

and the irreducible susceptibility $\chi_{\boldsymbol{q}}^0$ is

$$\chi_{\boldsymbol{q}}^0(\omega_l) = -\frac{T}{N}\sum_{\boldsymbol{k},n} G_{\boldsymbol{q}+\boldsymbol{k}}(\omega_l+\epsilon_n) G_{\boldsymbol{k}}(\epsilon_n), \tag{5}$$

where Matsubara frequencies are denoted by $\epsilon_n=(2n+1)\pi T$ and $\omega_l=2l\pi T$, respectively.

The self-energy is given by

$$\Sigma_{\boldsymbol{k}}(\epsilon_n) = \frac{T}{N}\sum_{\boldsymbol{q},l} G_{\boldsymbol{k}-\boldsymbol{q}}(\epsilon_n-\omega_l) V_{\boldsymbol{q}}(\omega_l), \tag{6}$$

where the effective interaction $V_{\boldsymbol{q}}$ is

$$V_{\boldsymbol{q}}(\omega_l) = U^2\left(\tfrac{3}{2}\chi_{\boldsymbol{q}}^s(\omega_l) + \tfrac{1}{2}\chi_{\boldsymbol{q}}^c(\omega_l) - \chi_{\boldsymbol{q}}^0(\omega_l)\right) + U. \tag{7}$$

We calculate Green's function self-consistently with Dyson's equation,

$$G_{\boldsymbol{k}}(\epsilon_n)^{-1} = i\epsilon_n + \mu - \epsilon_{\boldsymbol{k}}^0 - \Sigma_{\boldsymbol{k}}(\epsilon_n). \tag{8}$$

The irreducible particle-hole vertex $\Gamma_{\boldsymbol{k}\boldsymbol{k}'}^I$ which satisfies $\Gamma_{\boldsymbol{k}\boldsymbol{k}'}^I(\epsilon_n,\epsilon_{n'}) = \delta\Sigma_{\boldsymbol{k}}(\epsilon_n)/\delta G_{\boldsymbol{k}'}(\epsilon_{n'})$ is given by

$$\Gamma_{\boldsymbol{k}\boldsymbol{k}'}^I(\epsilon_n,\epsilon_{n'}) = V_{\boldsymbol{k}-\boldsymbol{k}'}(\epsilon_n-\epsilon_{n'}), \tag{9}$$

where the Maki-Thompson term is taken into account and the Aslamazov-Larkin term is omitted because the latter is negligible for the CVC.[19]

In this paper we take $N=N_x\times N_y\times N_z=64\times 64\times 32$ $\boldsymbol{k}$-point meshes and the Matsubara frequencies $\epsilon_n$ take the value from $-(2N_c-1)\pi T$ to $(2N_c-1)\pi T$ with $N_c=256$.

### B. Conductivity

In order to derive the transport coefficient, we begin with Kubo formula,

$$\sigma_{\mu\nu} = e^2\sum_{\boldsymbol{k}\boldsymbol{k}'\sigma\sigma'} v_{\boldsymbol{k}\mu}^0 v_{\boldsymbol{k}'\nu}^0 \left.\frac{\mathrm{Im}\,K_{\boldsymbol{k}\sigma,\boldsymbol{k}'\sigma'}(\omega+i\delta)}{\omega}\right|_{\omega=0}, \tag{10}$$

where $K(\omega+i\delta)$ is analytic continuation of below $K(i\omega)$,

$$K_{\boldsymbol{k}\sigma,\boldsymbol{k}'\sigma'}(i\omega_n) = \int_0^\beta d\tau e^{\omega_n \tau} \langle T_\tau \{ c^\dagger_{\boldsymbol{k}\sigma}(\tau) c_{\boldsymbol{k}\sigma}(\tau) c^\dagger_{\boldsymbol{k}'\sigma'} c_{\boldsymbol{k}'\sigma'} \} \rangle, \tag{11}$$

and

$$v^0_{\boldsymbol{k}\mu} = \frac{\partial \epsilon^0_{\boldsymbol{k}}}{\partial k_\mu}. \tag{12}$$

Eliashberg[29] derived the conductivity in this way. By generalizing Eliashberg's theory[19,22] the conductivity is obtained as

$$\sigma_{xx} = e^2 \sum_{\boldsymbol{k}} \int \frac{d\epsilon}{\pi} \left( -\frac{\partial f}{\partial \epsilon} \right) \{ v_{\boldsymbol{k}x}(\epsilon) |G^R_{\boldsymbol{k}}(\epsilon)|^2 J_{\boldsymbol{k}x}(\epsilon) - \mathrm{Re}[G^R_{\boldsymbol{k}}(\epsilon)^2] \mathbf{v}_{\boldsymbol{k}x}(\epsilon)^2 \}, \tag{13}$$

$$\mathbf{v}_{\boldsymbol{k}}(\epsilon) = \boldsymbol{\nabla} [\epsilon^0_{\boldsymbol{k}} + \mathrm{Re}\, \Sigma_{\boldsymbol{k}}(\epsilon)], \tag{14}$$

where $\mathbf{v}_{\boldsymbol{k}}$ is the quasi-particle velocity (without $Z$-factor) and the retarded Green's function $G^R_{\boldsymbol{k}}(\epsilon)$ is derived by the analytic continuation. The total current $\boldsymbol{J}_{\boldsymbol{k}}$ is given by the Bethe-Salpeter equation

$$\boldsymbol{J}_{\boldsymbol{k}}(\epsilon) = \mathbf{v}_{\boldsymbol{k}}(\epsilon) + \sum_{\boldsymbol{k}'} \int_{-\infty}^{\infty} \frac{d\epsilon'}{4\pi i} \mathcal{T}^I_{22}(\boldsymbol{k}\epsilon, \boldsymbol{k}'\epsilon') |G^R_{\boldsymbol{k}'}(\epsilon')|^2 \boldsymbol{J}_{\boldsymbol{k}'}(\epsilon'), \tag{15}$$

which is based on the Ward identity. The irreducible four-point vertex $\mathcal{T}^I_{lm}(\boldsymbol{k}\epsilon, \boldsymbol{k}'\epsilon')$ is defined in Ref. 29. According to Eq. (9), it is given by

$$\mathcal{T}^I_{22}(\boldsymbol{k}\epsilon, \boldsymbol{k}'\epsilon') = \left( \mathrm{cotanh}\, \frac{\epsilon' - \epsilon}{2T} - \tanh \frac{\epsilon'}{2T} \right) \times 2i\, \mathrm{Im}\, V_{\boldsymbol{k}'-\boldsymbol{k}}(\epsilon' - \epsilon + i\delta). \tag{16}$$

### C. Hall coefficient

When a weak magnetic field $B$ is induced along the $z$ axis, the Hall coefficient $R_H$ is given by

$$R_H = \frac{\sigma_{xy}/B}{\sigma_{xx}\sigma_{yy}}. \tag{17}$$

The Hall conductivity $\sigma_{xy}$ is obtained by[19,30]

$$\sigma_{xy}/B = -e^3 \sum_{\boldsymbol{k}} \int \frac{d\epsilon}{2\pi} \left( -\frac{\partial f}{\partial \epsilon} \right) |\mathrm{Im}\, G^R_{\boldsymbol{k}}(\epsilon)| |G^R_{\boldsymbol{k}}(\epsilon)|^2 A_{\boldsymbol{k}}(\epsilon), \tag{18}$$

$$A_{\boldsymbol{k}}(\epsilon) = v_{\boldsymbol{k}x}(\epsilon) \left[ J_{\boldsymbol{k}x}(\epsilon) \frac{\partial J_{\boldsymbol{k}y}(\epsilon)}{\partial k_y} - J_{\boldsymbol{k}y}(\epsilon) \frac{\partial J_{\boldsymbol{k}x}(\epsilon)}{\partial k_y} \right] + \langle x \leftrightarrow y \rangle, \tag{19}$$

where $f(\epsilon) = 1/(\exp(\epsilon/T) + 1)$.

### D. Nernst effect

Nernst coefficient under a weak magnetic field $B$ along $z$ axis and gradient of temperature along $x$ axis is defined as

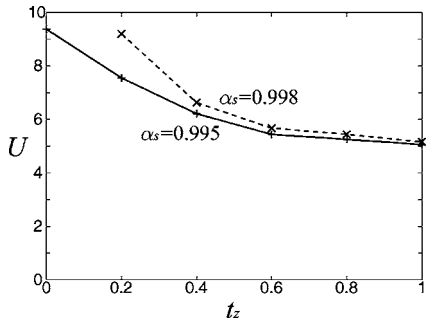


FIG. 2. $U$ against $t_z$ for $\alpha_S = 0.995$ (solid line) and $\alpha_S = 0.998$ (dotted line) at $T = 0.02$.

$$\nu = \frac{-E_y}{B \partial_x T}. \tag{20}$$

According to the linear response theory,[31] the response function $L^{21}_{\mu\nu}$ is defined as

$$L^{21}_{\mu\nu}(i\omega_l) = -\frac{T}{\omega_l} \int_0^\beta d\tau e^{i\omega\tau} \langle T_\tau j^Q_\mu(\tau) j_\nu(\tau = 0) \rangle. \tag{21}$$

The electron current operator $\boldsymbol{j}$ and the heat current operator $\boldsymbol{j}^Q$ are given by

$$\boldsymbol{j} = e \sum_{\boldsymbol{k},\sigma} \mathbf{v}^0_{\boldsymbol{k}} c^\dagger_{\boldsymbol{k},\sigma} c_{\boldsymbol{k},\sigma}, \tag{22}$$

and

$$\boldsymbol{j}^Q(\omega_l) = \lim_{\tau' \to \tau} \sum_{\boldsymbol{k},\sigma} \int_0^\beta d\tau e^{i\omega_l \tau} \frac{1}{2} \left( \frac{\partial}{\partial \tau} - \frac{\partial}{\partial \tau'} \right) c^\dagger_{\boldsymbol{k},\sigma}(\tau) c_{\boldsymbol{k},\sigma}(\tau') \tag{23}$$

$$= \frac{T}{N} \sum_{\boldsymbol{k},n,\sigma} i(\epsilon_n + \omega_l/2) \boldsymbol{v}^0_{\boldsymbol{k}} c^\dagger_{\boldsymbol{k},\sigma}(\epsilon_n) c_{\boldsymbol{k},\sigma}(\epsilon_n + \omega_l), \tag{24}$$

respectively.

After the analytic continuation for Eq. (21), $L^{21}_{xx}$ and $L^{21}_{xy}$ are obtained as[32]

$$L^{21}_{xx}(+i\delta) = eT \sum_{\boldsymbol{k}} \int \frac{d\epsilon}{\pi} \left( -\frac{\partial f}{\partial \epsilon} \right) \boldsymbol{q}_{\boldsymbol{k}x}(\epsilon) \times \{ |G^R_{\boldsymbol{k}}(\epsilon)|^2 J_{\boldsymbol{k}x}(\epsilon) - \mathrm{Re}[G^R_{\boldsymbol{k}}(\epsilon)^2] \boldsymbol{v}_{\boldsymbol{k}x}(\epsilon) \}, \tag{25}$$

$$L^{21}_{xy}(+i\delta) = BTe^2 \sum_{\boldsymbol{k}} \int \frac{d\epsilon}{\pi} \left( -\frac{\partial f}{\partial \epsilon} \right) |\mathrm{Im}\, G^R_{\boldsymbol{k}}(\epsilon)| |G^R_{\boldsymbol{k}}(\epsilon)|^2 A'_{\boldsymbol{k}}(\epsilon), \tag{26}$$

$$\gamma_{\boldsymbol{k}}(\epsilon) = -\,\mathrm{Im}\, \Sigma_{\boldsymbol{k}}(\epsilon), \tag{27}$$

$$A'_{\boldsymbol{k}}(\epsilon) = \gamma_{\boldsymbol{k}}(\epsilon) \left\{ \boldsymbol{Q}_{\boldsymbol{k}}(\epsilon) \times [\boldsymbol{v}_{\mathbf{k}}(\epsilon) \times \boldsymbol{\nabla}]_z \left[ \frac{\boldsymbol{J}_{\boldsymbol{k}}(\epsilon)}{\gamma_{\boldsymbol{k}}(\epsilon)} \right] \right\}_z, \tag{28}$$

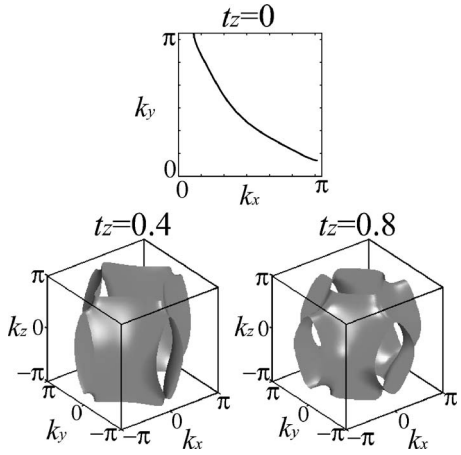


FIG. 3. Fermi surface for 2D with $t_z=0$ (upper panel), q3D with $t_z=0.4$ (lower left panel), and 3D with $t_z=0.8$ (lower right panel) for $T=0.02$, $\alpha_S=0.995$.

$$\boldsymbol{Q}_{\boldsymbol{k}}(\epsilon)=\boldsymbol{q}_{\boldsymbol{k}}(\epsilon)+\sum_{\boldsymbol{k}'}\int\frac{d\epsilon'}{4\pi i}\mathcal{T}^{I}_{22}(\boldsymbol{k}\epsilon,\boldsymbol{k}'\epsilon')|G^{R}_{\boldsymbol{k}'}(\epsilon')|^2\boldsymbol{Q}_{\boldsymbol{k}'}(\epsilon'), \tag{29}$$

where $\boldsymbol{q}_{\boldsymbol{k}}$ is the quasiparticle heat velocity $\mathrm{q}_{\boldsymbol{k}}(\epsilon)=\epsilon\boldsymbol{v}_{\boldsymbol{k}}(\epsilon)$.

Using above expressions, $\nu$ can be rewritten as

$$\nu=\frac{L^{21}_{xy}}{BT^2\sigma_{xx}}-\frac{S\sigma_{xy}}{B\sigma_{xx}}, \tag{30}$$

where the thermopower $S$ is given by

$$S=\frac{1}{T^2}\frac{L^{21}_{xx}}{\sigma_{xx}}. \tag{31}$$

## III. RESULT

Here, we show numerical results obtained by the CVC-FLEX approximation. We use filling $n=0.9$ ($n=1$ corresponds to half filling) and the intralayer hopping parameters $t_1=1$, $t_2=-1/6$, and $t_3=1/5$, which reproduce the Fermi surface of 2D high-$T_c$ cuprate YBCO, and introduce the interlayer hopping $t_z$ which makes the Fermi surface three-dimensional. The Stoner factor $\alpha_S=\max\{U\chi^0_{\mathbf{q}}(\omega=0)\}$ represents the "distance" from the AF order ($\alpha_S=1$ corresponds to the boundary of the AF or the spin density wave order) since the denominator of the static spin susceptibility is $1-U\chi^0$. We calculate for each $t_z$ with keeping $\alpha_S$, by tuning the value of $U$ as shown by a solid line for $\alpha_S=0.995$ and dotted line for $\alpha_S=0.998$ at $T=0.02$ in Fig. 2. The "distance" from the AF order is considered to be same along these lines. Note that $\alpha_S<1$ is always satisfied in 2D ($t_z=0$) at finite temperatures reflecting the theory of Mermin-Wagner.[33]

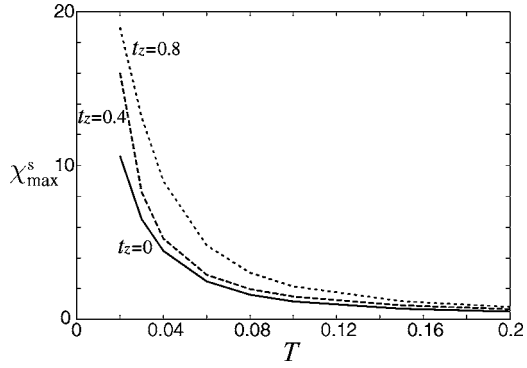


FIG. 5. The temperature dependence of the peak value of spin susceptibility for $t_z=0$, 0.4, 0.8, in the condition of $\alpha_S=0.995$ at $T=0.02$.

Figure 3 shows the Fermi surface for $t_z=0$ (2D), $t_z=0.4$ (quasi-3D; q3D) and $t_z=0.8$ (3D). We see that three dimensionality becomes stronger as the value of $t_z$ increases. The $\boldsymbol{k}$ dependence of the static spin susceptibility $\chi^s_{\boldsymbol{k}}$ is shown in Fig. 4, where the peak position is commensurate; $(k_x,k_y)=(\pi,\pi)$ for $t_z=0$ (2D), $(k_x,k_y,k_z)=(\pi,\pi,\pi)$ for $t_z=0.4$ (q3D), and incommensurate around $(\pi,\pi,\pi)$ for $t_z=0.8$ (3D). From these peak structures, we ensure that the AF fluctuations are dominant in these systems. In this case, the peak values of $\chi^s$ increase with $t_z$ as seen in Fig. 5. This means that the present system approaches the AF instability as the dimensionality changes from 2D to 3D.

To understand 3D structure of the relaxation time $\tau$, we show the $\boldsymbol{k}$ dependence of $\gamma_{\boldsymbol{k}}(=-\mathrm{Im}\,\Sigma_{\boldsymbol{k}}(\epsilon=0))\propto 1/\tau_{\boldsymbol{k}}$ along the Fermi surface in Figs. 6–8 where hot spots are depicted by circles and cold spots are illustrated by dotted circle. The bottom panels represent the momentum dependence of $\gamma_{\boldsymbol{k}}$ along the Fermi surface for each $k_z$. We see the hot spots exist on the plains of $k_z=0$ and $k_z=\pi/4$ for $t_z=0.4$ and $t_z=0.8$, respectively.

The volume fraction of hot spots decreases as $t_z$ increases, and for the three-dimensional case ($t_z=0.8$) hot spots have point-like structure ("hot points"), which is consistent with the experimental result obtained by de Haas-van Alphen measurements on $CeIn_3$.[34] Generally in 3D systems, nesting exists in only small parts of the Fermi surface, and hot spots form there. In general, the "hot lines"[7] where hot spots form

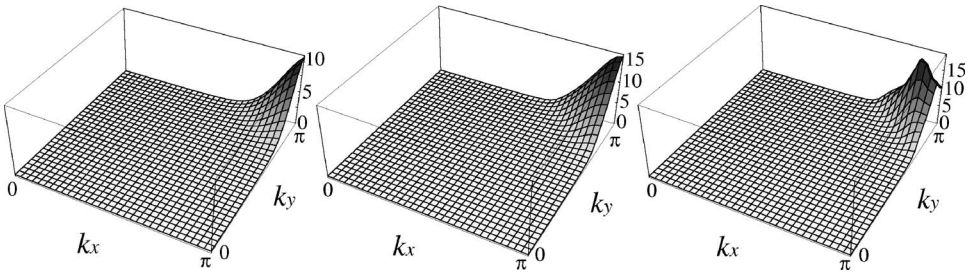


FIG. 4. The spin susceptibility for $t_z=0$ (left panel), 0.4 (middle panel) with $k_z=\pi,0.8$ (right panel) with $k_z=\pi$, for $\alpha_S=0.995$, $T=0.02$.

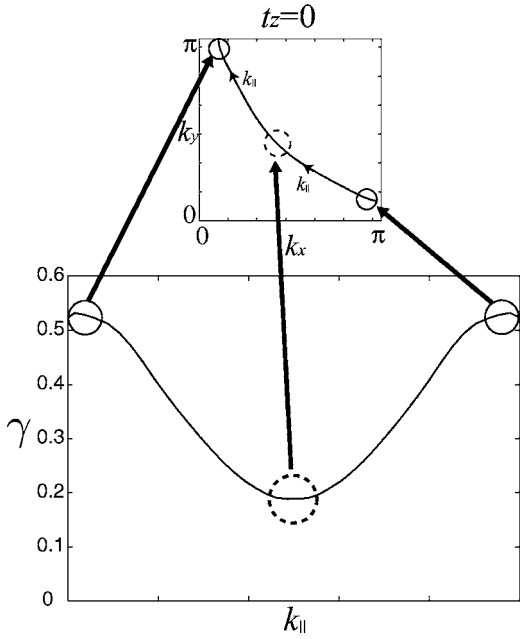


FIG. 6. $\gamma$ along the Fermi surface for $t_z=0$, $\alpha_S=0.995$ at $T=0.02$, where the hot spots and cold spots are depicted by solid circles and dotted circle, respectively.

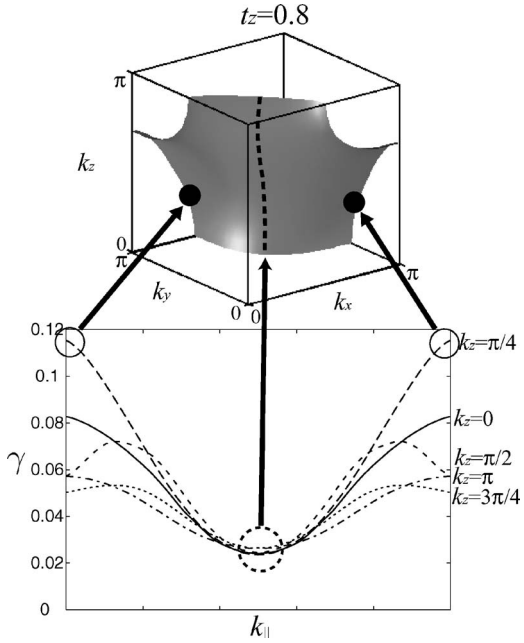


FIG. 8. $\gamma$ along the Fermi surface for $t_z=0.8$, $\alpha_S=0.995$, at $T=0.02$ where the hot spots and the cold lines are depicted by circles and dotted thick line, respectively.

line-like structure would not be appropriate in 3D systems.

On the other hand, $\gamma_k$ increases more sharply along $k_\parallel$ direction than $k_z$ direction around minimum point of $\gamma_k$ for $t_z=0.4$ and 0.8 as depicted in Figs. 7 and 8. In this sense, cold spots stretch strikingly along the $k_z$ direction. Then, cold spots form line-like structure ("cold lines"). They are aligned perpendicular to the plain with hot spots. The formation of hot points and cold lines would be generally expected in three-dimensional systems. To confirm the generality, we must study much more systems with various types of 3D Fermi surfaces.

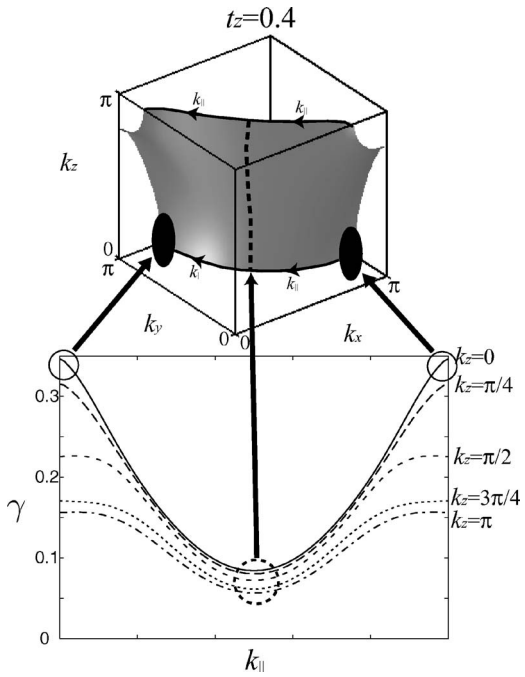


FIG. 7. $\gamma$ along the Fermi surface for $t_z=0.4$, $\alpha_S=0.995$ at $T=0.02$, where the hot spots and the "cold lines" are depicted by circles and a dotted thick line, respectively. The trajectories of $k_\parallel$ are depicted on the Fermi surface in $k_z=0,\pi$ as examples.

The calculated temperature dependence of the resistivity $\rho=1/\sigma_{xx}$ for $t_z=0$ (2D), $t_z=0.4$ (q3D), and $t_z=0.8$ (3D) with $U=9.4$, $U=6.2$, and $U=5.2$, respectively (see Fig. 2), are shown in Fig. 9, where the unit of $\rho$ is $\hbar a_c/e^2 \sim 2.4 \times 10^{-6}\ \Omega\,\mathrm{m}$ for a bilayer YBCO (lattice constant along $c$ axis: $a_c=5.8\times10^{-10}$ m) and $3.1\times10^{-6}\ \Omega\,\mathrm{m}$ for $CeCoIn_5$ ($a_c=7.6\times10^{-10}$ m), respectively. The value of $U$ is chosen to satisfy $\alpha_S=0.995$ at $T=0.02$ for each case. In this case, the "distance" from the AF QCP is the same among three $t_z$ parameters. We see that, independent of the dimensionality, the resistivities with and without the CVC are proportional to the temperature. Then, the value of $\rho$ is slightly enhanced by

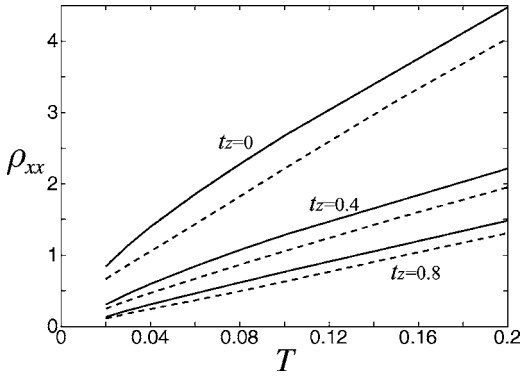


FIG. 9. The resistivity $\rho$ with the CVC (solid line) and without the CVC (dotted line) for $t_z=0$, 0.4, 0.8 as a function of $T$ with $\alpha_S=0.995$ at $T=0.02$.

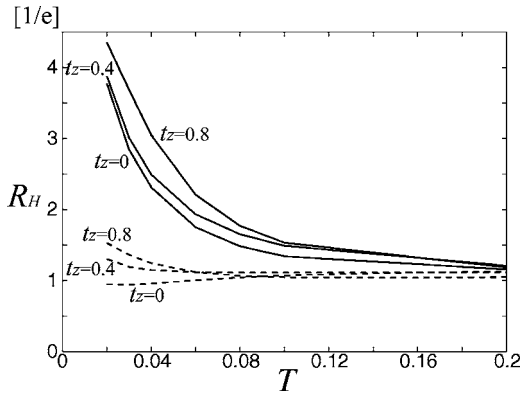


FIG. 10. The Hall coefficient $R_H$ with the CVC (solid line) and without the CVC (dotted line) for $t_z$=0, 0.4, 0.8 as a function of $T$, with $\alpha_S$=0.995 at $T$=0.02.

the CVC. It decreases as $t_z$ increases since the corresponding value of $U$ is reduced. This $T$-linear behavior of the resistivity is consistent with experiments for the systems close to the AF QCP, such as two-dimensional high-$T_c$ cuprate and three-dimensional $CeCoIn_5$.[2] In detail, the resistivities with the CVC show sublinear temperature dependence in low temperatures, which are also observed in the experimental results for heavy fermion $CeRhIn_5$ (private discussion). According to the SCR theory,[15,35] the resistivity behaves as $\rho \propto T$ in 2D, and $\rho \propto T^{3/2}$ in 3D. However, the SCR theory also predicts that $\rho \propto T$ for a wide range of temperatures even in 3D systems when the system is close to the AF QCP, which is consistent with the present numerical calculation.

Next, we show the temperature dependence of the Hall coefficient $R_H$ in Fig. 10, where the unit of $R_H$ is $a_a a_b a_c/e \sim 5.2\times10^{-10}$ m$^3$/C for a bilayer YBCO (lattice constant along $a$ and $b$ axies: $a_a=a_b=3.8\times10^{-10}$ m and that along $c$ axis: $a_c=5.8\times10^{-10}$ m) and $1.0\times10^{-9}$ m$^3$/C for $CeCoIn_5$ ($a_a=a_b=4.6\times10^{-10}$ m and $a_c=7.6\times10^{-10}$ m), respectively. In regard to the horizontal axis, unit of the temperature $t_1$ is 4000 K for YBCO. On the other hand, we estimate the nearest-neighbor hopping $t_1$=400 K for $CeCoIn_5$, because the experimetal data[2] show that magnitude of $R_H$ begins to increase below 40 K, which corresponds to $0.1t_1$ in Fig. 10. The $R_H$ without the CVC, which corresponds to the RTA, is almost constant. However, independent of the dimensionality, $R_H$ with the CVC increases as temperature decreases, which is consistent with experimental results for high-$T_c$ cuprate[36] and heavy fermion compounds ($CeCoIn_5$,[2] $CeCu_{6-x}Au_x$,[4] and $YbRh_2Si_2$—Ref. 5). Namely, the RTA cannot explain the strong temperature dependence of the Hall coefficient close to the AF QCP. Moreover, in the 3D case hot spots take point-like shape, which means that the effective electron density for transport phenomena ($n_{\rm eff}$) is large compared with two-dimensional case.[37] Since $R_H^{\rm RTA} \approx 1/en_{\rm eff}$ is satisfied in the RTA, $R_H^{\rm eff}$ cannot become large in 3D systems.

As a result, the CVC is indispensable to explain the behavior of $R_H$ in 3D close to the AF QCP. In the present results, the maximum enhancement of $R_H$ is given by $R_H(T=0.02)/R_H(t=0.2)\sim5$ for $t_z$=0.8 and $\alpha_S$=0.998. $R_H$ should increase further if we calculate at lower temperatures. The

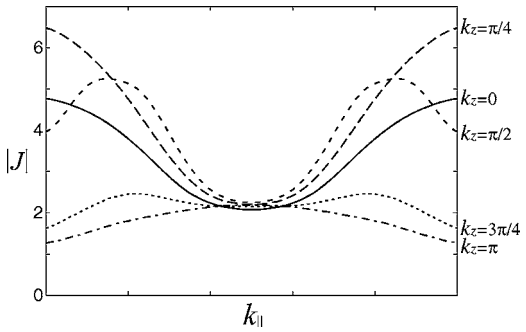


FIG. 11. Absolute value of the total current $\boldsymbol{J}$ with the CVC along the Fermi surface for $t_z$=0.8 and $t_z$=0 (thin line) with $\alpha_S$ =0.995 at $T$=0.02.

shape of the Fermi surface in $CeCoIn_5$ resembles that of our model for $t_z$=0.8. However, to reproduce the experimental results in $CeCoIn_5$ quantitatively, we have to study it based on the realistic band structures of $CeCoIn_5$.[38,39] Our calculation shows that $R_H$ is strongly enhanced by the CVC even in 3D systems, and its maximum value becomes as large as that in 2D.

Here, we discuss the reason why $R_H$ is strongly enhanced by the CVC in 3D systems based on the numerical study. The general expression for $\sigma_{xy}$ is given by[30,40]

$$\sigma_{xy}/B = -\frac{e^3}{8\pi}\int dk_z \oint_{\rm FS} dk_\parallel |\boldsymbol{J}_{\boldsymbol{k}}|_\perp^2 \left(\frac{\partial\theta_{\boldsymbol{J}}(\boldsymbol{k})}{\partial k_\parallel}\right)\frac{1}{(\gamma_{\boldsymbol{k}})^2}, \quad (32)$$

where $k_\parallel$ is the component of $\boldsymbol{k}$ along the unit vector $\boldsymbol{e}_\parallel(\boldsymbol{k}) = (\boldsymbol{e}_z\times\boldsymbol{v}_{\boldsymbol{k}})/|\boldsymbol{v}_{\boldsymbol{k}}|$ which is in the $k_xk_y$ plane and parallel to the Fermi surface. $|\boldsymbol{J}_{\boldsymbol{k}}|_\perp=\sqrt{J_{\boldsymbol{k}x}^2+J_{\boldsymbol{k}y}^2}$, and $\theta_{\boldsymbol{J}}$ is the angle between the total current $\boldsymbol{J}$ and the $x$ axis. In this line integration $\boldsymbol{k}$ point moves counterclockwise along the Fermi surface around the $k_z$ axis.

We see that for $t_z$=0.8, cold spots (where $\gamma_{\boldsymbol{k}}$ is small) form lines (cold lines) at the center of the Fermi surface along the $z$ axis in Fig. 8. As shown in the last term of Eq. (32), the main contribution for $\sigma_{xy}$ is expected to come from the cold lines. We see that in Fig. 11 the momentum depen-

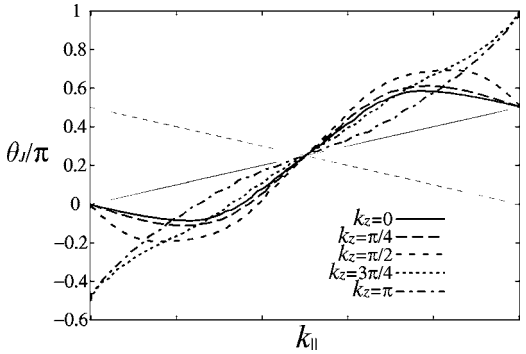


FIG. 12. The angle $\theta_{\boldsymbol{J}}$ of the total current $\boldsymbol{J}$ with the CVC along the Fermi surface for $t_z$=0.8, $\alpha_S$=0.995 at $T$=0.02. Thin line and dotted thin line approximately correspond to the angle $\theta_{\boldsymbol{v}}$ of the current without the CVC for $k_z=0-\pi/2$ and $k_z=3\pi/4-\pi$, respectively.

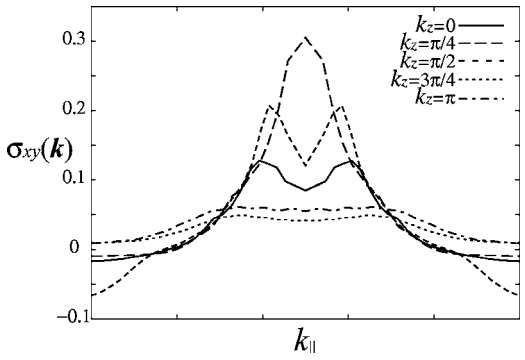


FIG. 13. $\sigma_{xy}(\boldsymbol{k})$ along the Fermi surface for $t_z=0.8$, $\alpha_S=0.995$ at $T=0.02$.

dence of the absolute value of the total current $|\boldsymbol{J}_k|$ is quite similar to that of $\gamma_k$.

In Fig. 12, we plot $\theta_J$ along the trajectories of $k_\parallel$. As references, we also plot the corresponding quantity without the CVC, $\theta_{\mathbf{v}}$ for $k_z=0-\pi/2$ and $k_z=3\pi/4-\pi$ as a thin line and a dotted thin line, respectively. As show in Fig. 12, $\theta_{\mathbf{v}}$ for $k_z=0-\pi/2$ and $k_z=3\pi/4-\pi$ decrease and increase, respectively, along the trajectories of $k_\parallel$. On the other hand, $\theta_J$ has a nonmonotonic change along these trajectories. In particular, for $k_z=3\pi/4-\pi$ $\theta_J$ decreases contrary to the case of $\theta_{\mathbf{v}}$. We stress that the magnitude of $\partial\theta_J/\partial k_\parallel$ becomes larger than that without the CVC ($\partial\theta_v/\partial k_\parallel$) around the cold lines.

In Fig. 13, we plot the momentum resolved Hall conductivity $\sigma_{xy}(\boldsymbol{k})$ defined by $\sigma_{xy}=\Sigma_{\boldsymbol{k}}\sigma_{xy}(\boldsymbol{k})$, where $\sigma_{xy}(\boldsymbol{k})$ is given by $\sigma_{xy}(\boldsymbol{k})=-\int(d\epsilon/2\pi N)(-\partial f/\partial\epsilon)|\mathrm{Im}\, G_{\boldsymbol{k}}^R(\epsilon)||G_{\boldsymbol{k}}^R(\epsilon)|^2A_{\boldsymbol{k}}(\epsilon)$. The magnitude of $\sigma_{xy}(\boldsymbol{k})$ takes large values around the cold lines, especially for $k_z=-\pi/2-\pi/2$. We should comment that for $k_z=3\pi/4,\pi$ the difference of the value of $\theta_{\boldsymbol{v}}$ and $\theta_J$ becomes $\pi$ at the edge of the trajectory as shown in Fig. 12 due to the CVC. At that time, the direction of $\boldsymbol{J}_k$ is opposite to that of $\boldsymbol{v}_k$. In this case, strong AF spin fluctuation enhances the magnitude of $\mathcal{T}_{22}^1(\boldsymbol{k}\epsilon,\boldsymbol{k}'\epsilon')$ in Eq. (15) for $\boldsymbol{k}-\boldsymbol{k}'=\pm(\pi,\pi,\pi)$, $\pm(-\pi,\pi,\pi)$, $\pm(\pi,-\pi,\pi)$, and $\pm(\pi,\pi,-\pi)$. In this case, from Eq. (15), we can obtain $\boldsymbol{J}_k\approx\boldsymbol{v}_k+\alpha_k\boldsymbol{J}_{k'}$ $(0<\alpha\leqslant 1)$.[19] This equation is easily solved as

$$\boldsymbol{J}_k=\frac{\boldsymbol{v}_k+\alpha_k\boldsymbol{v}_{k'}}{1-\alpha_k\alpha_{k'}}. \tag{33}$$

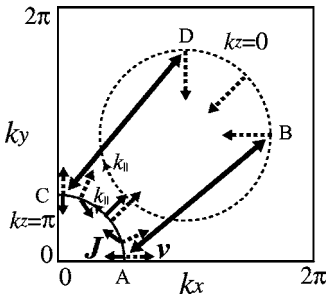


FIG. 14. Schematic illustration to show that at $A$ and $B$ $\boldsymbol{J}_k$ can direct opposite to $\boldsymbol{v}_k$, where the Fermi surface for $k_z=0,\pi$ is depicted by dotted and solid circle, respectively, and $\boldsymbol{J}_k$ and $\boldsymbol{v}_k$ are depicted by solid and dotted arrows, and the thick left-right arrows represent the coupling points.

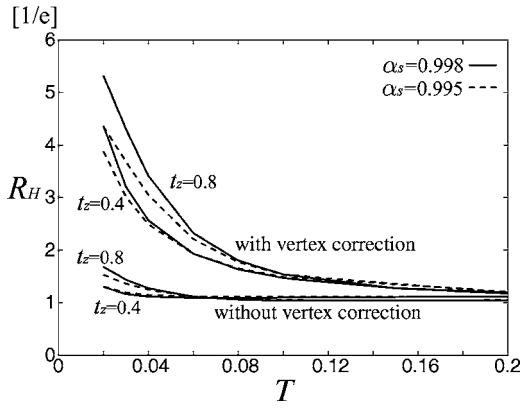


FIG. 15. The Hall coefficient $R_H$ with the CVC (upside) and without the CVC (downside) for $t_z=0.4$, 0.8 as a function of $T$ with $\alpha_S=0.995$ (solid line), 0.998 (dotted line) at $T=0.02$.

In Fig. 14, we illustrate schematic behaviors of the quasiparticle velocity $\boldsymbol{v}_k$ and the total current $\boldsymbol{J}_k$ on the Fermi surfaces sliced at $k_z=\pi$ (solid circle) and at $k_z=0$ (dotted circle). We focus on the position of points $A$ and $B$, which are connected by the nesting vector $\boldsymbol{k}-\boldsymbol{k}'=(-\pi,-\pi,\pi)$. Here, we write the quasiparticle velocities at $A$ and $B$ as $\boldsymbol{v}_k$ and $\boldsymbol{v}_{k'}$, respectively. We see that $\boldsymbol{v}_k$ and $\boldsymbol{v}_{k'}$ are antiparallel and $|\boldsymbol{v}_k|<|\boldsymbol{v}_{k'}|$. Considering that $\alpha\lesssim 1$, $\boldsymbol{J}_k$ given in Eq. (33) takes an opposite direction of $\boldsymbol{v}_k$. In the same way, the total current and the quasiparticle velocity at $C$ are also antiparallel. This nontrivial behavior of $\boldsymbol{J}_k$ has not been pointed out in previous studies for two-dimensional systems. This feature might induce an anomalous transport phenomenon.

In Fig. 15, we show the temperature dependence of $R_H$ for $\alpha_S=0.998$ (solid line) and $\alpha_S=0.995$ (dotted line) for $t_z=0.4$ and 0.8. We see that $R_H$ with the CVC increases as $\alpha_S$ approaches unity. It seems that $R_H$ tends to diverge as the system approaches the AF QCP. The reason can be understood by seeing Fig. 16, where $\partial\theta_{\mathbf{J}}/\partial k_\parallel$ takes a large value at the cold spot which corresponds to the center of the $k_\parallel$ axis. According to Eq. (32), this fact leads to the strong enhancement of $\sigma_{xy}$.

Finally, we discuss the Nernst coefficient $\nu$. It is known that $\nu$ vanishes in a complete spherical system, which is

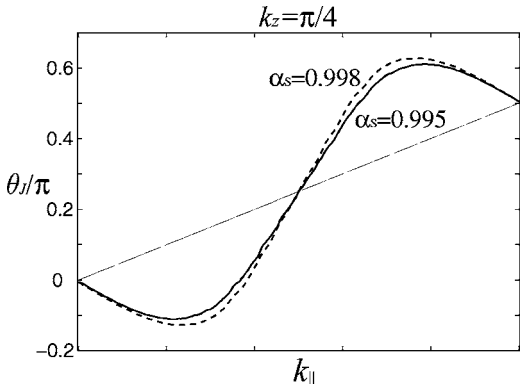


FIG. 16. The angle $\theta_J$ of the total current $\boldsymbol{J}$ with the CVC along the Fermi surface for $t_z=0.8$, $k_z=\pi/4$, $\alpha_S=0.995$ (solid line), and $\alpha_S=0.998$ (dotted line) at $T=0.02$. The thin line approximately corresponds to one without the CVC.

called Sondheimer cancellation.[12,41] Although this cancellation is not perfect in real anisotropic systems, the magnitude of $\nu$ becomes small ($\sim$1 nV/kT) in conventional metals.

However, $\nu$ is enhanced below $T^*$ (in the pseudogap region) for high-$T_c$ cuprates. The authors of Refs. 41 and 42 suggest a possibility that the vortex-like excitation emerges in under-doped high-$T_c$ cuprates to explain the enhancement of $\nu$ in the pseudogap region.

On the other hand, A.K.[21,43] has shown that strong enhancement of $\nu$ for high-$T_c$ cuprates is naturally derived based on the FLEX+T-matrix approximation with the CVC. Furthermore, $CeCoIn_5$ also shows huge *negative* $\nu$ below 20 K,[3] which cannot be ascribed to the vortex mechanism. Here, we aim to reveal the mechanism of the unconventional enhancement for $\nu$ close to the QCP irrespective of the dimensionality.

We estimate the renormalization factor ($z$) dependence of the transport coefficients, before showing the result of $\nu$. In the following, we will show that $\rho$ and $R_H$ are independent of $z$, and $\nu \propto z^{-1}$ in Hubbard model. Using the relation[32]

$$\sum_{\boldsymbol{k}} = \frac{1}{(2\pi)^3}\int dS_{\boldsymbol{k}} dk_\perp = \frac{1}{(2\pi)^3}\int \frac{dS_{\boldsymbol{k}} d\epsilon^0_{\boldsymbol{k}}}{|\boldsymbol{v}^0_{\boldsymbol{k}}|} = \frac{1}{(2\pi)^3}\int \frac{dS_{\boldsymbol{k}} d\epsilon^*_{\boldsymbol{k}}}{z|\boldsymbol{v}_{\boldsymbol{k}}|}, \tag{34}$$

where $S_{\boldsymbol{k}}$ is the Fermi surface and $k_\perp$ represents the momentum perpendicular to the Fermi surface and also using the relation $|G^R_{\boldsymbol{k}}(\epsilon)|^2 \sim \pi z \delta(\epsilon - \epsilon^*_{\boldsymbol{k}})/\gamma_k$ ($\epsilon^*_{\boldsymbol{k}} = z(\epsilon^0_{\boldsymbol{k}} + \mathrm{Re}\Sigma_{\boldsymbol{k}}(0) - \mu)$) for $\gamma \ll T$, we obtain

$$\sigma_{xx} \sim \frac{e^2}{(2\pi)^3}\int \frac{dS_{\boldsymbol{k}} d\epsilon^*_{\boldsymbol{k}}}{z|\boldsymbol{v}_{\boldsymbol{k}}|}\left(-\frac{\partial f}{\partial \epsilon}\right)_{\epsilon=\epsilon^*_{\boldsymbol{k}}} \boldsymbol{v}_{kx}\boldsymbol{J}_{kx}\frac{z}{\gamma_{\boldsymbol{k}}} \tag{35}$$

$$\propto (z)^0. \tag{36}$$

In the same way, $\sigma_{xy}$ is given by

$$\sigma_{xy} \sim \frac{e^3 B}{4(2\pi)^3}\int \frac{dS_{\boldsymbol{k}} d\epsilon^*_{\boldsymbol{k}}}{z|\boldsymbol{v}_{\boldsymbol{k}}|}\left(-\frac{\partial f}{\partial \epsilon}\right)_{\epsilon=\epsilon^*_{\boldsymbol{k}}} A_{\boldsymbol{k}}\frac{z}{\gamma^2_{\boldsymbol{k}}} \tag{37}$$

$$\propto (z)^0. \tag{38}$$

We see that $\sigma_{xx}$ and $\sigma_{xy}$ are independent of $z$. Thus, we confirm that $\rho = 1/\sigma_{xx} \propto (z)^0$ and $R_H = \sigma_{xy}/B\sigma^2_{xx} \propto (z)^0$ are independent of $z$. On the other hand, thermopower $S$ is given by

$$S \sim \frac{e}{(2\pi)^3 T\sigma_{xx}}\int \frac{dS_{\boldsymbol{k}} d\epsilon^*_{\boldsymbol{k}}}{z|\boldsymbol{v}_{\boldsymbol{k}}|}\left(-\frac{\partial f}{\partial \epsilon}\right)_{\epsilon=\epsilon^*_{\boldsymbol{k}}} \epsilon^*_{\boldsymbol{k}}\boldsymbol{v}_{kx}\boldsymbol{J}_{kx}\frac{z}{\gamma_{\boldsymbol{k}}} \tag{39}$$

$$= \frac{e}{(2\pi)^3 T\sigma_{xx}}\int \frac{dS_{\boldsymbol{k}} d\epsilon^*_{\boldsymbol{k}}}{z|\boldsymbol{v}_{\boldsymbol{k}}|}\left(-\frac{\partial f}{\partial \epsilon}\right)_{\epsilon=\epsilon^*_{\boldsymbol{k}}} (\epsilon^*_{\boldsymbol{k}})^2\frac{\partial}{\partial k_\perp}\left(\frac{\boldsymbol{v}_{kx}\boldsymbol{J}_{kx}}{|\boldsymbol{v}_{\boldsymbol{k}}|\gamma_{\boldsymbol{k}}}\right)_{\epsilon=0} \tag{40}$$

$$= \frac{e\pi^2 k_B^2 T}{3(2\pi)^3\sigma_{xx}}\int \frac{dS_{\boldsymbol{k}}}{z|\boldsymbol{v}_{\boldsymbol{k}}|}\frac{\partial}{\partial k_\perp}\left(\frac{\boldsymbol{v}_{kx}\boldsymbol{J}_{kx}}{|\boldsymbol{v}_{\boldsymbol{k}}|\gamma_{\boldsymbol{k}}}\right)_{\epsilon=0} \tag{41}$$

$$\propto z^{-1}, \tag{42}$$

and using $Q_k \sim \boldsymbol{q}_{\boldsymbol{k}} = \epsilon \boldsymbol{v}_{\boldsymbol{k}}$ for $T \to 0$, $\alpha_{xy} = L^{21}_{xy}(+i\delta)/T^2$ is given by

$$\alpha_{xy} \sim \frac{Be^2}{2(2\pi)^3 T}\int \frac{dS_{\boldsymbol{k}} d\epsilon^*_{\boldsymbol{k}}}{z|\boldsymbol{v}_{\boldsymbol{k}}|}\left(-\frac{\partial f}{\partial \epsilon}\right)_{\epsilon=\epsilon^*_{\boldsymbol{k}}} \epsilon^*_{\boldsymbol{k}} A''_{\boldsymbol{k}}(\epsilon^*_{\boldsymbol{k}})\frac{z}{\gamma^2_{\boldsymbol{k}}} \tag{43}$$

$$= \frac{Be^2}{2(2\pi)^3 T}\int \frac{dS_{\boldsymbol{k}} d\epsilon^*_{\boldsymbol{k}}}{z|\boldsymbol{v}_{\boldsymbol{k}}|}\left(-\frac{\partial f}{\partial \epsilon}\right)_{\epsilon=\epsilon^*_{\boldsymbol{k}}} (\epsilon^*_{\boldsymbol{k}})^2\frac{\partial}{\partial k_\perp}\left(\frac{A''_{\boldsymbol{k}}}{|\boldsymbol{v}_{\boldsymbol{k}}|\gamma^2_{\boldsymbol{k}}}\right)_{\epsilon=0} \tag{44}$$

$$= \frac{Be^2\pi^2 k_B^2 T}{6(2\pi)^3}\int \frac{dS_{\boldsymbol{k}}}{z|\boldsymbol{v}_{\boldsymbol{k}}|}\frac{\partial}{\partial k_\perp}\left(\frac{A''_{\boldsymbol{k}}}{|\boldsymbol{v}_{\boldsymbol{k}}|\gamma^2_{\boldsymbol{k}}}\right)_{\epsilon=0} \tag{45}$$

$$\propto z^{-1}, \tag{46}$$

where $A''_{\boldsymbol{k}}(\epsilon)$ is defined by

$$A''_{\boldsymbol{k}}(\epsilon) = \gamma_{\boldsymbol{k}}(\epsilon)\left\{\boldsymbol{v}_{\boldsymbol{k}}(\epsilon)\times[\boldsymbol{v}_{\boldsymbol{k}}(\epsilon)\times\nabla]_z\left[\frac{\boldsymbol{J}_{\boldsymbol{k}}(\epsilon)}{\gamma_{\boldsymbol{k}}(\epsilon)}\right]\right\}_z. \tag{47}$$

Thus, we obtain $\nu = \alpha_{xy}/B\sigma xx - S\sigma_{xy}/B\sigma_{xx} \propto z^{-1}$. We must consider $z$ in detail to calculate $\nu$, because $z$ is much smaller in heavy fermion systems. From the experiment of de Haas-van Alphen,[44] we can estimate that the effective mass $m^* \sim 100m_0$ ($m_0$ is the bare electron mass) and the mass obtained by the band calculation $m_b \sim 2m_0$ in branches $\beta$. Then, the mass enhancement factor $z^{-1}$ is given by $z^{-1} = m^*/m_b \sim 50$.

Although the FLEX can describe various critical phenomena near the AF QCP, the mass enhancement is not completely explained with the FLEX in heavy fermion systems. The reason is that local correlations are not fully taken into account in the framework of the FLEX, because the vertex corrections in the self-energy are not included. According to Ref. 45, we separate the self-energy into the "local part" and the "nonlocal part." In this case, total renormalization factor $z$ is obtained as $z = z_0 z^*$, where $z_0$ is the local renormalization factor which cannot be included in the FLEX and renormalization factor $z^* = (1 - (\partial\Sigma/\partial\omega))^{-1}$ is obtained by the FLEX. To fit the total renormalization factor to the experimental results ($z^{-1} = 50$), we use $z_0 = 3/50$, because $z^* \sim 1/3$ in our calculation.

We show the obtained temperature dependence of the Nernst coefficient $\nu$ in Fig. 17, where solid and dotted lines correspond to $\nu$ with and without the CVC, respectively, for $t_z = 0$, $t_z = 0.4$, and $t_z = 0.8$. In this figure, we chose the parameters for heavy fermion $CeCoIn_5$, i.e., $a_a = a_b = 4.6 \times 10^{-10}$ m, and then, $k_B a_a a_b/\hbar \sim 28$ nV/kT has been multiplied as a unit of calculated value, and the local mass enhancement factor $z_0^{-1}$ has also been multiplied.

We see that $\nu$ without the CVC is almost constant, and $\nu$ with the CVC shows enormous increase at low temperatures, especially in strong three-dimensional case ($t_z = 0.8$) where the Fermi surface is similar to that of $CeCoIn_5$. Then, the temperature dependence of $\nu$ resembles that of $R_H$. This temperature dependence of $|\nu|$ is consistent with the giant Nernst effect in $CeCoIn_5$ ($|\nu| \sim 1$ $\mu$V/kT for $T = 5$ K).[3] Here, we dis-

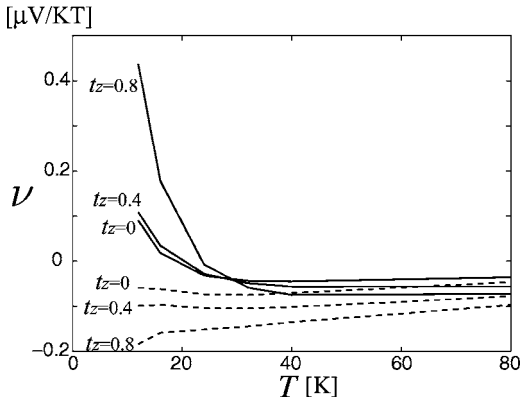


FIG. 17. The Nernst coefficient $\nu$ with the CVC (solid line) and without the CVC (dotted line) for $t_z$=0, 0.4, 0.8 as a function of $T$ with $\alpha_S$=0.995 at $T$=5 K.

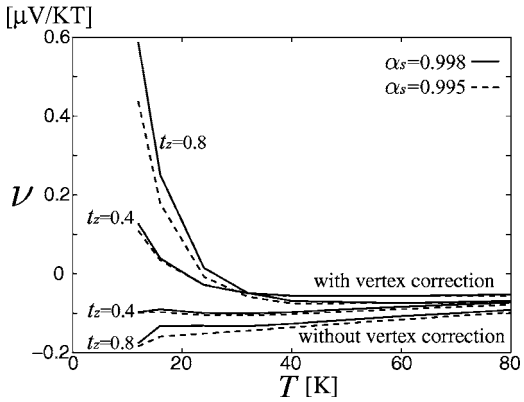


FIG. 18. The Nernst coefficient $\nu$ with the CVC (upside) and without the CVC (downside) for $t_z$=0.4, 0.8 as a function of $T$ with $\alpha_S$=0.995 (solid line) and 0.998 (dotted line) at $T$=5 K.

cuss the reason why the magnitude of $\nu$ becomes large. $A_{\boldsymbol{k}}$ and $A'_{\boldsymbol{k}}$ given in Eqs. (19) and (28) are rewritten as

$$A_{\boldsymbol{k}}(\epsilon) = |\boldsymbol{v}_{\boldsymbol{k}}(\epsilon)|_{\perp}\left(\boldsymbol{J}_{\boldsymbol{k}}(\epsilon) \times \frac{\partial}{\partial k_{\parallel}}\boldsymbol{J}_{\boldsymbol{k}}(\epsilon)\right)_z \tag{48}$$

$$= |\boldsymbol{v}_{\boldsymbol{k}}(\epsilon)|_{\perp}|\boldsymbol{J}_{\boldsymbol{k}}(\epsilon)|^2_{\perp}\frac{\partial\theta_{\boldsymbol{J}}(\boldsymbol{k})}{\partial k_{\parallel}}, \tag{49}$$

$$A'_{\boldsymbol{k}}(\epsilon) = \gamma_{\boldsymbol{k}}(\epsilon)|\boldsymbol{v}_{\boldsymbol{k}}(\epsilon)|_{\perp}\left(\boldsymbol{Q}_{\boldsymbol{k}}(\epsilon) \times \frac{\partial}{\partial k_{\parallel}}\frac{\boldsymbol{J}_{\boldsymbol{k}}(\epsilon)}{\gamma_{\boldsymbol{k}}(\epsilon)}\right)_z \tag{50}$$

$$= |\boldsymbol{v}_{\boldsymbol{k}}(\epsilon)|_{\perp}\left[(Q_{\boldsymbol{k}x}J_{\boldsymbol{k}x} + Q_{\boldsymbol{k}y}J_{\boldsymbol{k}y})\frac{\partial\theta_{\boldsymbol{J}}(\boldsymbol{k})}{\partial k_{\parallel}} + (\boldsymbol{Q}_{\boldsymbol{k}} \times \boldsymbol{J}_{\boldsymbol{k}})_z\frac{\partial}{\partial k_{\parallel}}\log\left(\frac{|\boldsymbol{J}_{\boldsymbol{k}}|_{\perp}}{\gamma_{\boldsymbol{k}}}\right)\right]. \tag{51}$$

Here, $\boldsymbol{Q}_{\boldsymbol{k}}$ is the total heat current with the CVC. We stress that $\boldsymbol{Q}_{\boldsymbol{k}} \sim \epsilon\boldsymbol{v}_{\boldsymbol{k}}$ and $\boldsymbol{Q}_{\boldsymbol{k}}$ is not parallel to $\boldsymbol{J}_{\boldsymbol{k}}$ when the AF fluctuations are strong.[21] In this case, $\nu$ is strongly enhanced due to the second term of $A'_{\boldsymbol{k}}$ in high-$T_c$ cuprates.[43] We expect that the same mechanism will give the enhancement of $\nu$ in the present study for three-dimensional case. In NCCO, $\nu$ is enhanced by the CVC due to the AF fluctuation below 300 K, whereas the increment of $\nu$ for LSCO is brought by the CVC due to both AF and superconducting fluctuations below $T^* \sim 150$ K.[21] Because of the relation $\nu \propto \gamma^{-1}$, $\nu$ is proportional to $\rho^{-1}$ for a fixed $\alpha_S$. This fact would contribute to the enhancement of $\nu$ in 3D case, as shown in Figs. 17 and 18. We show the temperature dependence of $\nu$ for both $\alpha_S$ =0.995 and 0.998 in Fig. 18. $\nu$ with the CVC increases as $\alpha_S$ approaches unity, which resembles the behavior of $R_H$. Consequently, the magnitude of $\nu$ increases almost divergently in the vicinity of the AF QCP.

## IV. CONCLUSION

We have calculated microscopically the resistivity $\rho$, the Hall coefficient $R_H$, and Nernst coefficient $\nu$ for three-dimensional Hubbard model close to the AF QCP based on the Fermi-liquid theory. This is a first microscopic calculation for the Hall coefficient and the Nernst coefficient with the current vertex corrections (CVC) in the three-dimensional system. In two-dimensional systems, it is established that the CVC plays an important role when the AF fluctuations are strong. On the other hand, the CVC vanishes completely in infinite dimension $d=\infty$. Thus, it is a very important theoretical issue to clarify whether the CVC is significant or not in three-dimensional systems. We find that the CVC influences crucially various transport phenomena in both two- and three-dimensional systems close to the AF QCP.

We have shown that the magnitude of $R_H$ and $\nu$ is strongly enhanced with the decrease of temperature due to the CVC. These strong temperature dependencies in the Hall coefficient and the Nernst coefficient come from the difference between the direction of the total current ($\boldsymbol{J}_{\boldsymbol{k}}$) and that of $\boldsymbol{v}_{\boldsymbol{k}}$ around the cold spots. The difference of directions increases as the temperature decreases near the QCP, which can be expressed in terms of the effective curvature $\partial\theta_{\boldsymbol{J}}/\partial k_{\parallel}$ of Fermi surface obtained by the direction of $\boldsymbol{J}_{\boldsymbol{k}}$. The obtained values of $R_H$ at the lowest temperature ($T$=0.02) are more than five times larger than those at high temperatures for three-dimensional system ($t_z$=0.8). This result is qualitatively consistent with experimental results in various three-dimensional heavy fermion systems close to the AF QCP, such as $CeCoIn_5$ and $CeCu_{6-x}Au_x$. This strong enhancement cannot be explained by the RTA.

In the present paper, we also studied the momentum dependence of relaxation time in three-dimensional systems due to strong AF spin fluctuations. In two-dimensional systems, it is known that hot spots and cold spots take line structures along $z$ axis, as the systems approach the AF QCP. In three-dimensional systems, we find that hot spots become point-like ("hot points") while the cold spots remain to take line structures ("cold lines"). The emergence of hot points and cold lines is expected to be general in three-dimensional systems close to the AF QCP. Transport phenomena are mainly determined by the cold spots. The area of cold spots in the phase space plays an important role. We find that the

CVC around cold spots produces strong enhancement of $R_H$ and $\nu$. We emphasize that the strong enhancement of $R_H$ and $\nu$ comes from the effective curvature of the Fermi surface, $\partial\theta_{\boldsymbol{J}}/\partial k_{\|}$, enhanced by the CVC on cold lines, as shown in Fig. 12. Note that obtained results for $R_H$ and $\nu$ without the CVC, which corresponds to the RTA, are almost temperature independent.

In the future, we will perform a quantitative study for the transport phenomena in $CeCoIn_5$ and $CeRhIn_5$, using a realistic band structure predicted by band calculations.[38,39] In the present paper, signs of $R_H$ and $\nu$ are opposite to actual experimental results. We expect that this discrepancy can be resolved by taking into account a proper band structure.

## ACKNOWLEDGMENTS

This work was supported by a Grant-in-Aid for 21st Century COE "Frontiers of Computational Science." Numerical calculations were performed at the supercomputer center, ISSP. The authors are grateful to K. Yamada, J. Inoue, N. Nagaosa, Y. Matsuda, Y. Suzumura, D. Hirashima, Y. Nakajima, and K. Tanaka for useful comments and discussions.

[1] C. Petrovic, P. G. Pagliuso, M. F. Hundley, R. Movshovich, J. L. Sarrao, J. D. Thompson, Z. Fisk, and P. Monthoux, J. Phys.: Condens. Matter **13**, L337 (2001).
[2] Y. Nakajima, K. Izawa, Y. Matsuda, S. Uji, T. Terashima, H. Shishido, R. Settai, Y. Onuki, and H. Kontani, J. Phys. Soc. Jpn. **73**, 5 (2004).
[3] R. Bel, K. Behnia, Y. Nakajima, K. Izawa, Y. Matsuda, H. Shishido, R. Settai, and Y. Onuki, Phys. Rev. Lett. **92**, 217002 (2004).
[4] T. Fukuhara, H. Takashima, K. Maezawa, and Y. Onuki (unpublished).
[5] S. Paschen, T. Lühmann, S. Wirth, P. Gegenwart, O. Trovarelli, C. Geibel, F. Steglich, P. Coleman, and Q. Si, Nature (London) **432**, 881 (2004).
[6] B. P. Stojković and D. Pines, Phys. Rev. B **55**, 8576 (1997).
[7] A. Rosch, Phys. Rev. B **62**, 4945 (2000).
[8] R. Hlubina and T. M. Rice, Phys. Rev. B **51**, 9253 (1995).
[9] J. M. Harris, Y. F. Yan, P. Matl, N. P. Ong, P. W. Anderson, T. Kimura, and K. Kitazawa, Phys. Rev. Lett. **75**, 1391 (1995).
[10] Y. Ando and T. Murayama, Phys. Rev. B **60**, R6991 (1999).
[11] H. Kontani, J. Phys. Soc. Jpn. **70**, 1873 (2001).
[12] E. H. Sondheimer, Proc. R. Soc. London, Ser. A **193**, 484 (1948).
[13] T. Moriya, Y. Takahashi, and K. Ueda, J. Phys. Soc. Jpn. **59**, 2905 (1990).
[14] K. Ueda, T. Moriya, and Y. Takahashi, J. Phys. Chem. Solids **53**, 1515 (1992).
[15] T. Moriya and K. Ueda, Adv. Phys. **49**, 555 (2000); Rep. Prog. Phys. **66**, 1299 (2003).
[16] N. E. Bickers, D. J. Scalapino, and S. R. White, Phys. Rev. Lett. **62**, 961 (1989).
[17] N. E. Bickers and D. J. Scalapino, Ann. Phys. (N.Y.) **193**, 206 (1989).
[18] P. Monthoux and G. G. Lonzarich, Phys. Rev. B **59**, 14598 (1999).
[19] H. Kontani, K. Kanki, and K. Ueda, Phys. Rev. B **59**, 14723 (1999).
[20] H. Kontani, J. Phys. Soc. Jpn. **70**, 2840 (2001).
[21] H. Kontani, Phys. Rev. Lett. **89**, 237003 (2002).
[22] H. Kontani and H. Kino, Phys. Rev. B **63**, 134524 (2001).
[23] A. Georges, G. Kotliar, W. Krauth, and M. J. Rozengerg, Rev. Mod. Phys. **68**, 13 (1996).
[24] G. Kotliar and D. Vollhardt, Phys. Today **57**, 53 (2004).
[25] S. Koikegami, S. Fujimoto, and K. Yamada, J. Phys. Soc. Jpn. **66**, 1438 (1997).
[26] H. Kontani and K. Ueda, Phys. Rev. Lett. **80**, 5619 (1998).
[27] G. Baym and L. P. Kadanoff, Phys. Rev. **124**, 287 (1961).
[28] G. Baym, Phys. Rev. **127**, 1391 (1962).
[29] G. M. Eliashberg, Zh. Eksp. Teor. Fiz. **41**, 410 (1961) [Sov. Phys. JETP **14**, 886 (1962)].
[30] H. Kohno and K. Yamada, Prog. Theor. Phys. **80**, 623 (1988).
[31] G. D. Mahan, *Many-Particle Physics*, 2nd ed. (Plenum, New York, 1990).
[32] H. Kontani, Phys. Rev. B **67**, 014408 (2003).
[33] N. D. Mermin and H. Wagner, Phys. Rev. Lett. **17**, 1133 (1966).
[34] T. Ebihara, N. Harrison, M. Jaime, S. Uji, and J. C. Lashley, Phys. Rev. Lett. **93**, 246401 (2004).
[35] T. Moriya and T. Takimoto, J. Phys. Soc. Jpn. **64**, 960 (1995).
[36] J. Takeda, T. Nishikawa, and M. Sato, Physica C **231**, 293 (1994).
[37] Y. Ōnuki, R. Settai, K. Sugiyama, T. Takeuchi, T. C. Kobayashi, Y. Haga, and E. Yamamoto, J. Phys. Soc. Jpn. **73**, 769 (2004).
[38] T. Maehira, T. Hotta, K. Ueda, and A. Hasegawa, J. Phys. Soc. Jpn. **72**, 854 (2003).
[39] Y. Haga, Y. Inada, H. Harima, K. Oikawa, M. Murakawa, H. Nakawaki, Y. Tokiwa, D. Aoki, H. Shishido, S. Ikeda, N. Watanabe, and Y. Onuki, Phys. Rev. B **63**, 060503(R) (2001).
[40] H. Fukuyama, H. Ebisawa, and Y. Wada, Prog. Theor. Phys. **42**, 494 (1969).
[41] Y. Wang, Z. A. Xu, T. Kakeshita, S. Uchida, S. Ono, Y. Ando, and N. P. Ong, Phys. Rev. B **64**, 224519 (2001).
[42] Z. A. Xu, N. P. Ong, Y. Wang, T. Kakeshita, and S. Uchida, Nature (London) **406**, 486 (2000).
[43] H. Kontani and K. Yamada, J. Phys. Soc. Jpn. **74**, 155 (2005).
[44] R. Settai, H. Shishido, S. Ikeda, Y. Murakawa, M. Nakashima, D. Aoki, Y. Haga, H. Harima, and Y. Ōnuki, J. Phys.: Condens. Matter **13**, L627 (2001).
[45] Y. Nishikawa, H. Ikeda, and K. Yamada, J. Phys. Soc. Jpn. **71**, 1140 (2002).